Reliable CNT thermoelectric modules enabled by flexible printed circuit board integration for self-powered IoT sensors

Horike, Shohei

Wei, Qingshuo

Synthetic Metals 317 (2026) 118086

Contents lists available at ScienceDirect

Synthetic Metals

journal homepage: www.elsevier.com/locate/synmet

Reliable CNT thermoelectric modules enabled by flexible printed circuit board integration for self-powered IoT sensors

Shohei Horike [a,b,c,d,**], Qingshuo Wei [d,e,*]

[a] Department of Chemical Science and Engineering, Graduate School of Engineering, Kobe University, 1-1 Rokkodai-cho, Kobe 657-8501, Japan
[b] Research Center for Membrane and Film Technology, Kobe University, 1-1 Rokkodai-cho, Kobe 657-8501, Japan
[c] Center for Environmental Management, Kobe University, 1-1 Rokkodai-cho, Kobe 657-8501, Japan
[d] Research Institute of Core Technology for Materials Innovation, Department of Materials and Chemistry, National Institute of Advanced Industrial Science and Technology (AIST), 1-1-1 Higashi, Tsukuba, Ibaraki 305-8565, Japan
[e] Graduate School of Pure and Applied Science, University of Tsukuba, 1-1-1 Tennodai, Tsukuba, Ibaraki 305-8577, Japan

ARTICLE INFO

Keywords:
Thermoelectric
Module
Carbon nanotube
Doping
Printed substrate

ABSTRACT

Carbon nanotube (CNT)-based thermoelectric (TE) materials have emerged as promising candidates for low-grade heat harvesting in self-powered Internet of Things (IoT) devices. However, the practical deployment of CNT-film TE modules has been hindered by two critical fabrication challenges, namely short circuits caused by the CNT whiskers that are generated during film dicing, and structural misalignment arising from manual stacking. In this study, a reliable TE module architecture is presented, which integrates n-type CNT films with a flexible printed circuit board (F-PCB) substrate, the latter of which functions simultaneously as an electrical interconnect and an effective insulating layer. A 50-pair TE module fabricated using this approach exhibited an open-circuit voltage of > 20 mV and a maximum output power of > 20 μW under a temperature difference of ~50 K. When connected to a commercial direct current (DC)-to-DC converter, the module successfully powered a Bluetooth Low Energy (BLE) temperature sensor, enabling real-time wireless data transmission to a smartphone. These results demonstrate that F-PCB-integrated CNT TE modules offer a high-yield, robust, and practical solution for sustainable self-powered IoT sensing technologies.

1. Introduction

The accelerated proliferation of wireless sensors and Edge Artificial Intelligence (AI) devices within the Internet of Things (IoT) ecosystem has created an urgent need for small, sustainable energy-harvesting technologies that can provide self-sufficient power at the point of use [1,2]. Projections indicate that the number of such deployed devices will reach the trillions. Powering such vast numbers of devices through conventional means (i.e., periodic battery replacement or extensive wired infrastructures), is not logistically or economically feasible in terms of maintenance, cost, or complexity.

Thermoelectric (TE) conversion, a form of energy harvesting that directly converts temperature differentials into electrical power, is a leading candidate for meeting this critical demand [3]. The Seebeck effect is the fundamental principle governing this technology, wherein a temperature difference (ΔT) across a conductive material promotes the diffusion of thermally activated charge carriers (electrons or holes) from the hotter end to the colder end [4]. This process generates an electromotive force (ΔV) proportional to the temperature difference, which is quantified by the Seebeck coefficient (S).

$$S = -\frac{\Delta V}{\Delta T}$$

The sign of S corresponds to the dominant carrier type of the material, i.e., positive for p-type materials where holes are the major carriers, and negative for n-type materials where electrons are the major carriers [5]. It is known that TE devices are capable of continuous power generation as long as a temperature gradient is maintained. Diverse potential heat sources are available for this purpose, including industrial

* Corresponding author at: Research Institute of Core Technology for Materials Innovation, Department of Materials and Chemistry, National Institute of Advanced Industrial Science and Technology (AIST), 1-1-1 Higashi, Tsukuba, Ibaraki 305-8565, Japan.
** Corresponding author at: Department of Chemical Science and Engineering, Graduate School of Engineering, Kobe University, 1-1 Rokkodai-cho, Kobe 657-8501, Japan.
E-mail addresses: horike@crystal.kobe-u.ac.jp (S. Horike), qingshuo.wei@aist.go.jp (Q. Wei).

https://doi.org/10.1016/j.synthmet.2026.118086
Received 2 December 2025; Received in revised form 15 January 2026; Accepted 20 January 2026
Available online 21 January 2026

waste heat, automotive exhaust, concentrated solar thermal energy, and even subtle heat dissipated from the human body. Since these heat sources are ubiquitous and nonintermittent, TE generation holds immense promise as a sustainable and decentralized power source.

Although inorganic semiconductors (such as bismuth telluride compounds) have traditionally dominated this field, organic TE materials have recently gained popularity [6,7]. The primary advantages associated with organic materials include their low-cost mass-production capability, light weight, mechanical flexibility, low toxicity, and ease of disposal (e.g., incineration). In particular, carbon nanotubes (CNTs) are highly promising primary constituents of high-performance organic TE materials because of their outstanding electrical conductivity, favorable Seebeck coefficient, and the ability to easily tune their polarity (p- or n-type) through chemical doping [8–10]. The resulting CNTs typically exhibit p-type polarity (positive S) owing to autoxidation in air. However, the incorporation of reducing chemicals with appropriate redox potentials, such as alkali metals [11], amines [12,13], superbases, phosphines [14] and crown ether complexes [15], can effectively produce n-type CNTs (with negative S) via electron-transfer interactions.

The electromotive force generated by a single TE element is typically in the microvolt-to-low-millivolt range under small temperature differences. Thus, to achieve a practical voltage sufficient for activating standard power management circuits, such as direct current (DC)-to-DC converters ($\geq$20 mV) [16,17], the construction of a TE module is necessary. In this configuration, p- and n-type elements, which generate voltages with opposite polarities when subjected to the same temperature gradient, are arranged thermally in parallel and electrically in series to sum their individual thermoelectromotive forces [18]. Therefore, the tunable CNT polarity is of paramount importance for the development of functional TE modules.

Previously, our group reported TE modules fabricated by alternately stacking polarity-controlled (chemically doped) self-standing CNT films with insulating films [19], achieving a high output power (~35 μW at $\Delta T = 40$ K), and successfully demonstrating the activation of a DC-to-DC converter to power a Bluetooth beacon. However, several critical challenges remain, particularly concerning the processing yield and structural reliability. Specifically, during dicing of the parent CNT film into individual TE elements, microscopic CNT fiber "whiskers" (burrs) inevitably form along the cut edges. These protruding fibers often create unintended electrical bridges between adjacent elements, leading to short circuits that severely reduce the overall thermoelectromotive force and power output. In a previous study, our group attempted to mitigate this issue by introducing a thick insulating layer and manually adjusting the position of the CNT film [19]. However, this manual alignment introduced cumulative stacking errors, resulting in a module that was not well aligned. Consequently, the final device exhibited uneven top and bottom surfaces. Such nonplanarity rendered the module unsuitable for applications requiring flat and stable thermal interfaces.

In this study, a novel fabrication method is proposed for TE modules, which fundamentally addresses the issue of short-circuiting that is commonly associated with CNT film processing. Specifically, a flexible printed circuit board (F-PCB) is introduced as a counterpart to the CNT-film TE element to suppress inter-element short circuits. It is expected that this approach will generate a high-voltage and high-reliability TE module that fully exploits the potential of high-performance CNT-based TE materials for use in IoT sensors.

2. Experimental

2.1. Film formation and chemical doping

Single-walled CNTs with a mean tube diameter of 1.6 nm were used for characterization and throughout the TE demonstrations. Self-standing CNT films (~70 mm diameter, ~30 μm thickness) were formed using an established procedure, as reported in our previous studies [19–23]. Specifically, CNT powder was ultrasonically dispersed in deionized water using a Brij L4 surfactant, which was vacuum-filtered through a polytetrafluoroethylene membrane filter. The CNT film was then detached from the filter, rinsed with deionized water and acetone, and air-dried overnight. The film was cut to the intended size (1×2 mm^2 for contact resistance measurements and 22×22 mm^2 for TE module fabrication). n-Type chemical doping was also performed according to the method developed in our previous study [19]. For this process, the organic superbase 1,5,7-triazabicyclo[4.4.0]dec-5-ene (TBD) was cross-linked using a decylene group to form 2TBD-C10, which served as an n-type inducer for the CNTs. 2TBD-C10 was dissolved in acetone, and the CNT films were immersed in the resulting solution prior to drying under vacuum. The obtained self-standing CNT films were then pressed under 5 MPa at 50 °C for 1 h to enhance film flatness prior to characterization and module fabrication.

2.2. TE module fabrication

The TE module was fabricated by alternately stacking the n-type CNT films and F-PCB substrates. This novel approach was designed to address the issue of short-circuiting caused by microscopic CNT whiskers during film dicing. The F-PCB substrate was used as a dual-function component, acting as both an electrical electrode and a robust insulator. The n-type CNT films, doped with 2TBD-C10, were initially pressed at 5 MPa and 50 °C for 1 h to enhance film flatness. Fifty elemental pairs (50 n-type CNT films and 50 F-PCB substrates) were stacked inside a jig with a 22 mm × 22 mm opening, eliminating the need for precise alignment. The stack was then pressed at 5 MPa and 50 °C for 1 h. After removal, the films were not fully densified but maintained sufficient contact. Finally, the module was fixed inside a plastic mold for measurement. In this configuration, the F-PCB connects the p- and n-type elements (p-type Cu electrode and n-type CNT film) thermally in parallel and electrically in series, summing their individual thermoelectromotive forces. No adhesion layer was used in this process [24,25].

2.3. Characterization

The film thickness was measured using a high-resolution digital measuring unit (VL-50-B, Mitutoyo). The electrical conductivities of the CNT films were determined using a four-probe conductivity meter (MCP-T600, Mitsubishi Chemical Corp.). All device-level electrical measurements were performed using a semiconductor parameter analyzer (4200-SCS, Keithley). The Seebeck coefficients were evaluated using a custom-built measurement system equipped with two Peltier modules (Ampere, UT40U100F) to generate controlled temperature differences. Microscopic observations of the CNT whiskers and film edges were performed using a digital microscope (VHX-7000; Keyence).

3. Results and discussion

In our previous work, dicing of the self-standing CNT films was found to generate microscopic CNT fiber whiskers along the cut edges. These protruding fibers created unintended electrical connections between adjacent CNT-TE elements—whether p–n, p–p, or n–n—resulting in short circuits that markedly reduced the overall thermoelectromotive force (ΔV). To directly evaluate this issue, high-resolution digital microscopy was employed, which enabled clear visualization of the whiskers (burrs) formed during the dicing process (Fig. 1a). The microscopy images revealed numerous CNT fibers extending from the cut surfaces, confirming that these otherwise hard-to-detect whiskers are the primary cause of electrical bridging and performance degradation in stacked CNT-film TE modules.

To resolve the yield limitation of whisker-induced short circuits, a novel approach was developed using F-PCB substrates to serve the crucial dual functions of an electrical electrode and a robust insulator.

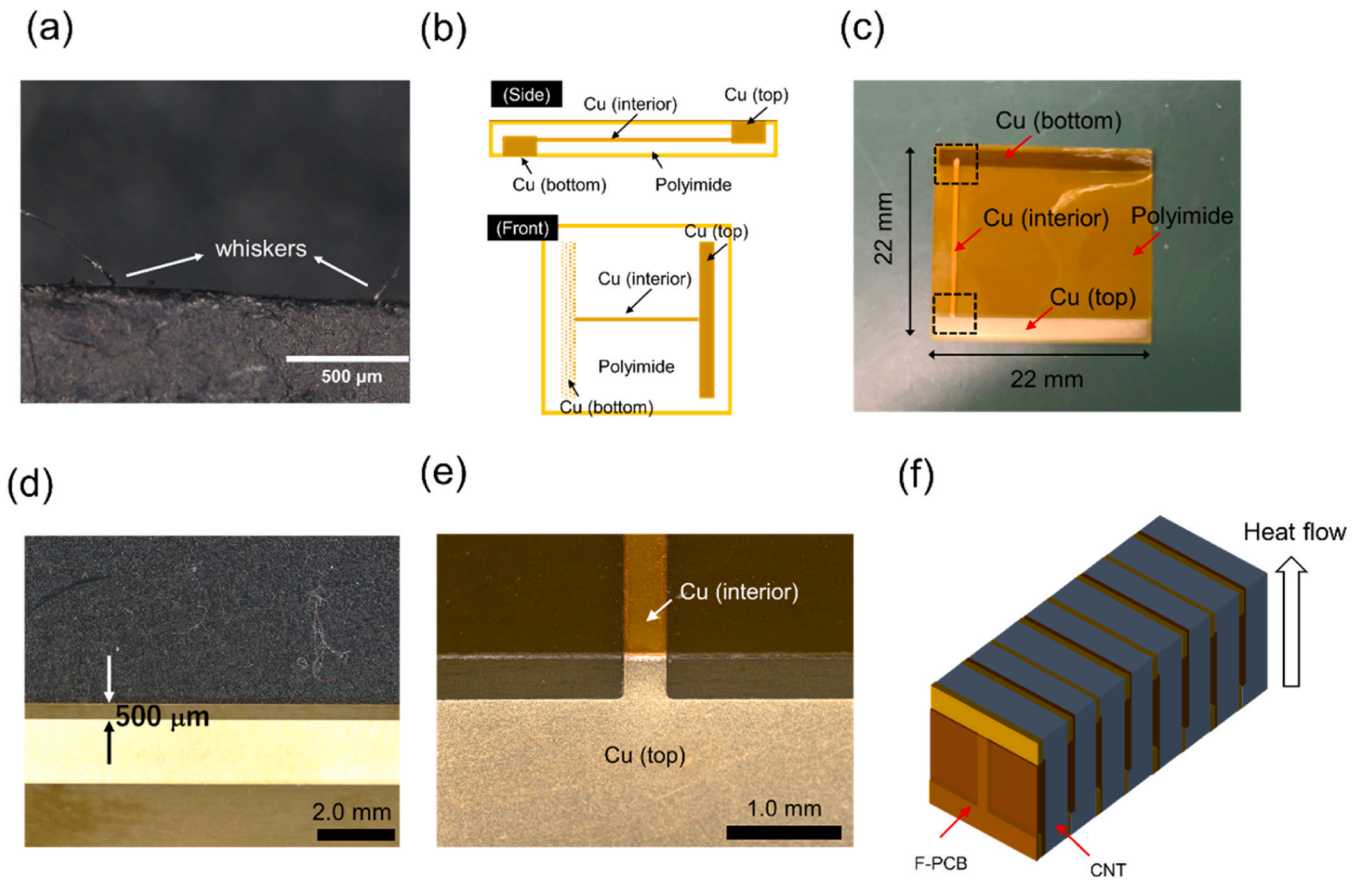

Fig. 1. (a) Digital microscopy image of a self-standing CNT film after dicing, showing the formation of microscopic CNT fiber whiskers (burrs) protruding from the cut edge. These whiskers are the primary cause of unintended electrical bridging between adjacent TE elements. (b) Schematic illustration and (c) photographic image of the flexible printed circuit board (F-PCB) structure used in this work, consisting of Cu electrodes patterned on both sides of a polyimide substrate, and interconnected through internal Cu traces. (d) Photographic image of the F-PCB substrate with Cu electrodes recessed 0.5 mm from the edge to avoid contact with the CNT burrs. (e) Enlarged view of the internal Cu electrode layout. (f) Schematic of the laminated thermoelectric modules used in this study, showing heat flow along the film direction.

As shown in Fig. 1b, the F-PCB was constructed from Cu electrodes on both sides of a polyimide film with identical dimensions to the CNT film (22 mm × 22 mm), wherein the top and bottom electrodes were electrically connected by internal Cu traces. The thickness of the Cu electrode was 18 μm.

The design parameters were carefully optimized to ensure reliable module performance. As shown in Fig. 1c, the electrode pattern maintains a 0.5 mm margin from the F-PCB edge to prevent short circuits caused by microscopic CNT burrs. In the current design, the p-type copper and n-type CNT films are intended to connect in series. However, CNT burrs can create unintended contact with copper at undesired locations. To avoid this, the copper electrode was positioned slightly inward so that any protruding burrs would touch the polyimide layer instead of copper, effectively eliminating shorting issues. The internal Cu wiring width was set to 0.4 mm (Fig. 1d), balancing the electrical and thermal conductivities of Cu and CNT films. Copper exhibits an electrical conductivity of ~59,000 S cm^{-1} and thermal conductivity of ~390 W m^{-1} K^{-1} , yielding a higher electrical-to-thermal conductivity ratio than CNT films (1000–2000 S cm^{-1} and 20–100 W m^{-1} K^{-1}). To minimize parasitic heat leakage while maintaining efficient electrical interconnection, the F-PCB adopts an I-shaped electrode design, reducing Cu cross-sectional area without compromising performance. When the CNT film thickness is comparable to Cu, the Cu provides superior electrical conductance and lower thermal conductance, acting as an efficient connector without significant heat loss. The top and bottom contact strips were each set to 2 mm to ensure low contact resistance, as discussed later.

The Seebeck coefficient of the Cu electrode on the F-PCB was measured by applying a controlled temperature difference of 0–7 K across the electrode, as shown in Fig. 2a. A stable stepwise voltage response was obtained, demonstrating that this measurement setup was sufficiently sensitive to resolve the extremely small thermoelectric signal generated by Cu. Although Cu exhibits a small intrinsic Seebeck coefficient of approximately + 3.9 μV K^{-1}, the positive and reproducible response observed here confirms its role as a stable p-type material (Fig. 2b) [26]. In contrast, 2TBD-C10-doped CNT films exhibited a negative stepwise voltage response (Fig. 2c), confirming n-type behavior, with an extracted Seebeck coefficient of approximately −25 μV K^{-1} (Fig. 2d). The electrical conductivity was about 1800 S cm^{-1}, and the calculated power factor reached 113 μW m^{-1} K^{-2}, consistent with previous studies [19]. This reliable thermoelectric performance ensures that the Cu electrode provides a consistent and effective electrical interface to the n-type CNT films in the module configuration.

Subsequently, the contact resistivity (ρ_c) between the CNT film and the Cu electrode was evaluated using the transmission line model (TLM), a standard method for quantifying interface-specific contact resistance [27]. In this technique, the total resistance (R) between the two contact pads was measured as a function of the separation distance (L). When R is plotted against L, the slope reflects the sheet resistance of the material beneath the contacts, whereas the vertical axis intercept corresponds to twice the contact resistance. In the current case, it was difficult to place Cu electrodes on the CNT films because of the multilayered structure on the rear side of the F-PCB substrate. Thus, as shown in Fig. 3a, the CNT films were laminated onto Cu electrodes after trimming the edges of the

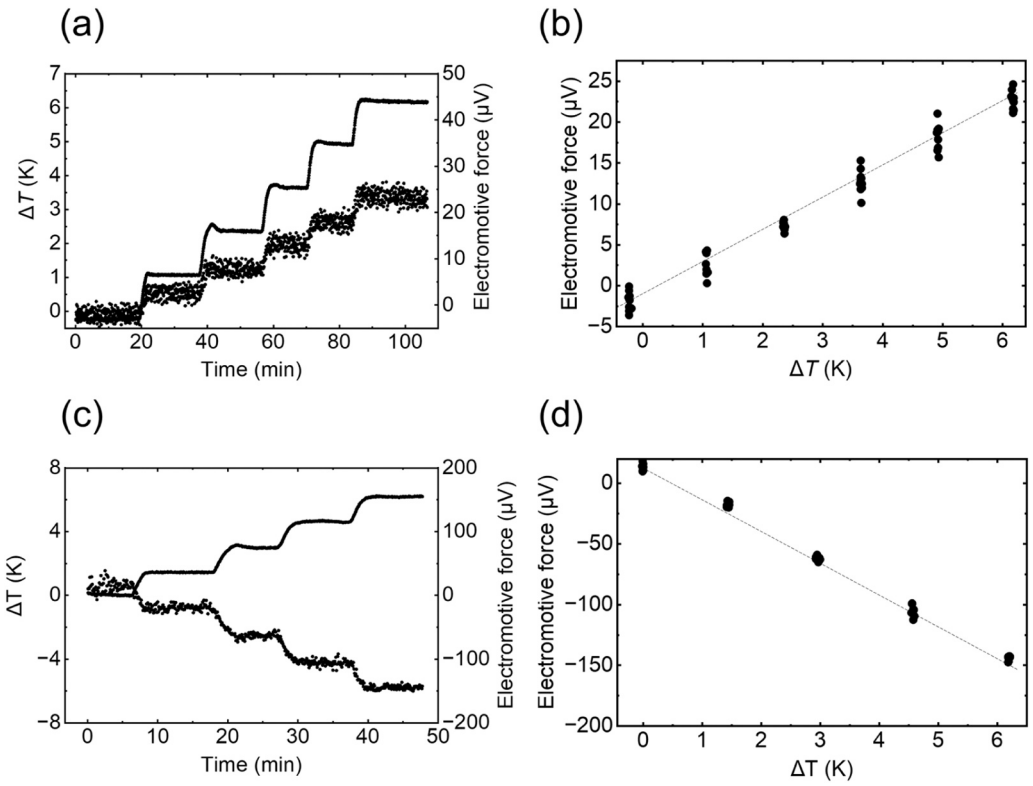

Fig. 2. Seebeck measurement results for the Cu electrode on the F-PCB and 2TBD-C10 doped CNT films. (a) Voltage response of the Cu electrode showing stable, stepwise changes corresponding to each applied temperature increment. (b) Extracted Seebeck coefficients for the Cu electrode, confirming a small but positive value of approximately + 3.9 μV K^{-1}; (a) Voltage response of the 2TBD-C10 doped CNT films. (b) Extracted Seebeck coefficients for the 2TBD-C10 doped CNT films, confirming a nagative value of approximately −25 μV K^{-1}.

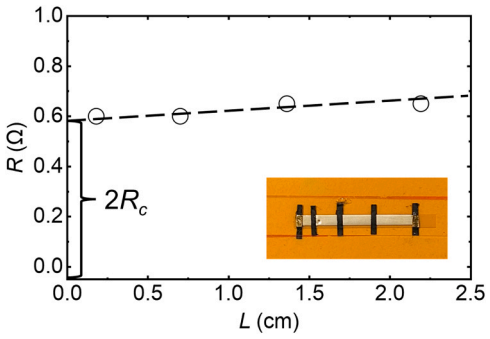

Fig. 3. TLM plot of the total resistance (*R*) versus the electrode spacing (*L*). The slope is effectively zero, reflecting the extremely low resistivity of Cu and confirming that the vertical-axis intercept originates almost entirely from the CNT/Cu contact. Inset: Photographic image of a CNT film laminated on the exposed Cu electrode.

F-PCB substrate. From Fig. 3b, it is apparent that the slope is zero, consistent with the extremely low resistivity of Cu, and indicating that the measured intercept originated almost entirely from the CNT/Cu interface. TLM analysis yielded a remarkably small contact resistivity of 0.6×10^4 μΩ cm^2, using the electrode area of 1×2 mm^2. This value is larger than those typically observed for inorganic semiconductor contacts (i.e., 10^0~10^2 μΩ cm^2) [28], but significantly smaller than those previously reported for conducting polymer–Au interfaces, thereby demonstrating excellent electrical compatibility between the CNT films and Cu electrodes. Using a contact area of 22×2 mm^2 (Fig. 1c), the corresponding contact resistance of only 0.01 Ω, indicates a negligible parasitic resistance contribution in the TE module.

To confirm the suppression of short circuits, a small-scale module configuration was evaluated. Fig. 4a shows that the alternate stacking of five n-type CNT films with four F-PCB substrates effectively sums the thermoelectromotive force from each element, achieving an aggregate Seebeck coefficient of ~95 μV K^{-1} (Fig. 4b and Fig. S1). Critically, this sum of the TE voltages was highly reproducible without any inter-element shorts, directly confirming the efficacy of the printed electrode substrate approach in addressing the fundamental fabrication challenge.

Building on the successful validation of short-circuit suppression and low contact resistance, a high-performance TE module was fabricated by alternately stacking 50 pairs of elements (50 n-type CNT films and 50 printed electrode substrates, Fig. 5a), with the cross-sectional microscopy images (Fig. 5b) revealing a distinct layered structure. The TE module exhibited a clear temperature-dependent performance trend under natural heat dissipation conditions, with both the open-circuit

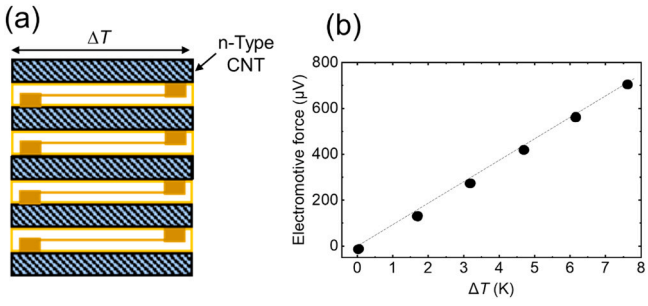

Fig. 4. (a) Schematic configuration of the small-scale TE module composed of five n-type CNT films alternately stacked with four F-PCB substrates. (b) Measured thermoelectromotive force for the stacked module, showing linear voltage summation from each CNT element and yielding an aggregate Seebeck coefficient of ~95 μV K^{-1}.

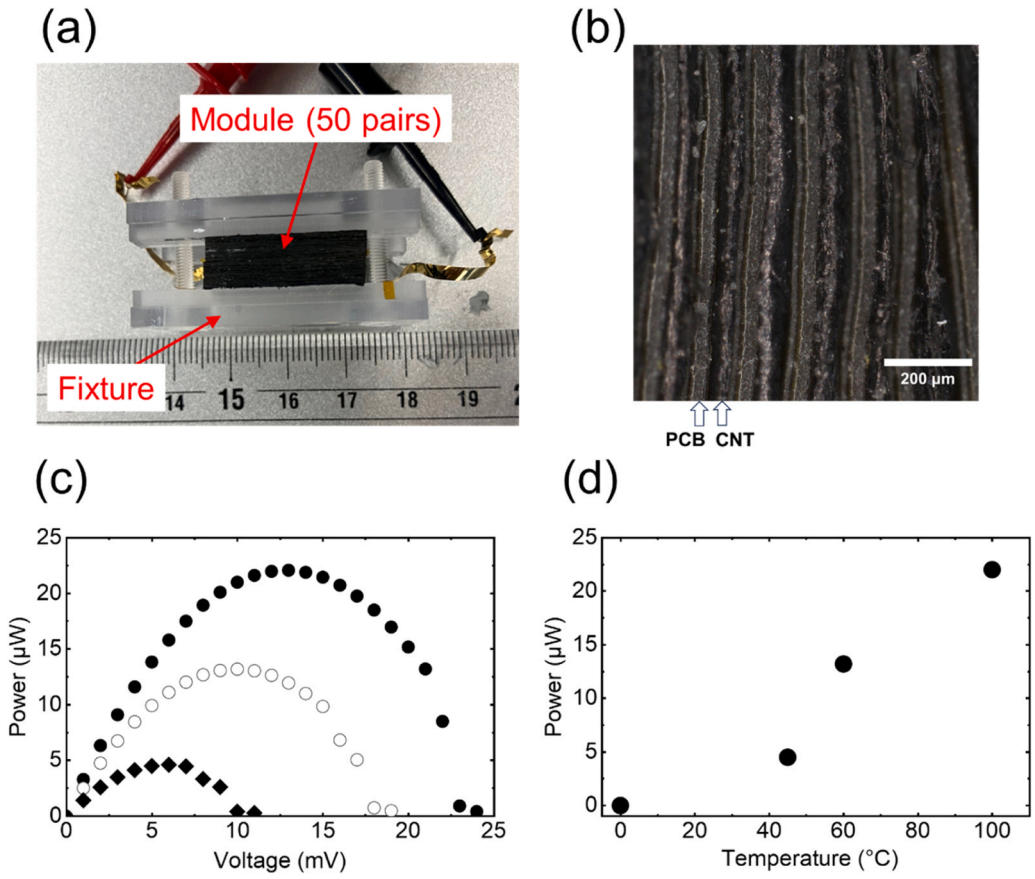

Fig. 5. (a) Photographic of the TE module composed of 50 n-type CNT films alternately stacked with 50 F-PCB substrates. (b) Cross-sectional microscopy image of the prepared TE module. (c) Temperature-dependent thermoelectric performance of the 50-pair module under natural heat dissipation conditions. (d) Maximum power output plotted as a function of the hot source temperature.

voltage (V_{OC}) and output power increasing steadily as the hot-side temperature increased from room temperature to 100 °C (Fig. 5c). The power output showed an approximately quadratic dependence on the temperature difference (ΔT), consistent with the theoretical expectation that power scales with $(\Delta T)^2$ due to the simultaneous increase in generated voltage and heat-driven charge transport (Fig. 5d). At a hot-side temperature of 100 °C, the module delivered a maximum output power of > 20 μW along with a V_{OC} of > 20 mV. This voltage level was sufficient to activate a standard DC-to-DC converter to power a Bluetooth Low Energy (BLE) sensor. We have fabricated and compared two modules using the same batch of CNT films, and their power output and internal resistance differed by about 20 %, indicating good reproducibility within a batch. When using different batches of n-type doped CNTs, the variation increased to more than 50 %, primarily due to slight

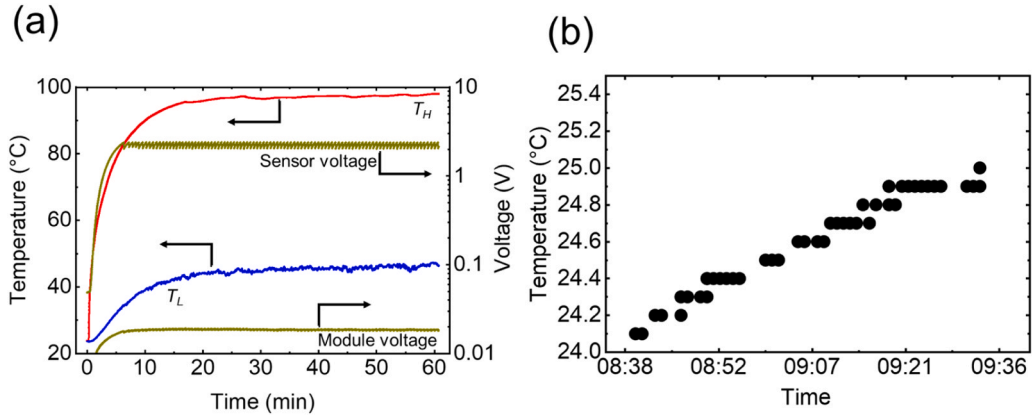

Fig. 6. (a) Demonstration of practical TE module operation under realistic conditions. The module was placed on a 100 °C heat source while the cold side was cooled naturally with a small heat sink. The cold-side temperature (T_L) gradually increased and stabilized at 45 −50 °C after ~30 min, establishing a steady temperature difference of ~50 K. Under this condition, the module output remained stable at ~20 mV, and was boosted to 2.4–2.2 V to power a BLE temperature sensor; each slight voltage drop corresponds to an individual wireless transmission event. (b) Air-temperature data transmitted wirelessly from the BLE sensor to a smartphone, recorded over a period of 1 h. The sensor delivers roughly 100 transmission events during this period, capturing a gradual increase in room temperature between 08:00 and 09:00.

differences in CNT properties and challenges in maintaining identical film thickness.

The practical capability of the TE module was evaluated under realistic operating conditions. As shown in Fig. 6a, the module was placed directly on a 100 °C heat source, while the cold side was allowed to dissipate heat naturally, aided by a small heat sink. Under these conditions, the cold-side temperature gradually increased and stabilized at ~45 −50 °C after ~30 min, establishing a steady temperature difference of ~50 K across the module. At this ΔT, the module generated a V_{OC} of > 20 mV, which was successfully boosted to > 2.4 V using an AP4473 DC-to-DC converter (Fig. 6a). This converted voltage was sufficient to drive the air-temperature sensor. Notably, the slight voltage drop shown in Fig. 6a corresponds to an individual wireless transmission event. The sensor continuously transmitted the air temperature data to a smartphone (Fig. 6b), where the recorded trend captured the gradual temperature increase in the room from 08:00–09:00. Within this 1 h measurement period, the system delivered ~100 transmission events, demonstrating stable and repeated operation. Based on the measured module performance, the estimated daily energy harvest is approximately 1.7 J (calculated as 20 μW × 3600 s × 24 h). This amount is significant compared to the typical power consumption of a BLE-based IoT sensor, which generally requires less than 10 mJ per data transmission [29]. Therefore, the harvested energy is sufficient to support intermittent sensor operation under these conditions. This confirms that the proposed module configuration can function reliably as a practical self-powered energy source for IoT-sensing devices in daily thermal environments.

The module exhibited good environmental and operational stability, maintaining consistent performance for over 150 h at 100°C under natural cooling conditions. It is worth noting that the loading resistance was 10 Ω, slightly different from the optimized condition. The fluctuations in power output were observed (Fig. 7), which were attributed to natural diurnal variations in ambient temperature rather than material degradation or device failure. Under certain room temperatures, the power output could nearly double, underscoring the critical role of cooling conditions. These results further confirm the reliability of the module and highlight its potential for energy harvesting in IoT sensor applications. We also summarized reported CNT-based and organic thermoelectric modules delivering more than 10 μW of output power, which we consider the minimum requirement for IoT sensors (Table S1). While our module does not exhibit the highest performance, its simple and scalable fabrication process makes this approach highly promising.

4. Conclusions

In this study, a reliable CNT-based TE module was developed by integrating n-type CNT films with an F-PCB substrate, which effectively addressed the well-known challenges of whisker-induced short circuits and structural misalignments in stacked CNT-film modules. Digital microscopy revealed the presence of microscopic CNT burrs formed during film dicing, which were the primary causes of inter-element electrical bridging in previous designs. By introducing the F-PCB as both an electrical interconnect and a robust insulating layer, shorting was successfully suppressed and a uniformly stacked modular structure was obtained. The CNT/Cu interface exhibited an exceptionally low contact resistivity, ensuring minimal parasitic loss and enabling efficient voltage summation across 50 TE pairs. As a result, the module delivered a maximum power output of > 20 μW and a V_{OC} of > 20 mV at a ΔT of ~50 K, which was sufficient to activate a commercial DC-to-DC converter. Furthermore, the continuous powering of a Bluetooth temperature sensor was demonstrated, achieving the successful transmission of data to a smartphone without the requirement for external power. These results confirm that the proposed fabrication strategy produces high-yield, mechanically robust, and practically deployable TE modules, thereby offering a promising pathway toward sustainable self-powered IoT sensor systems.

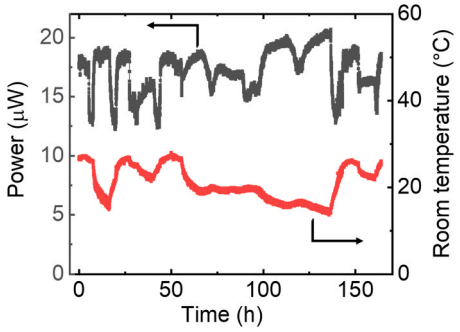

Fig. 7. Long-term stability of the module under natural air cooling with a 10 Ω resistive load. The hot-side temperature was maintained near 100 °C. Power output remained stable overall, with minor daily fluctuations due to diurnal ambient temperature changes.

Authors' statement

Q.W. and S.H. conceived the project and supervised this work. Q. W. performed the module fabrication and wrote the paper. S.H. supported the doping experiment and electrical conductivity measurements and the Seebeck coefficient measurements. Both authors discussed data and commented on the manuscript.

CRediT authorship contribution statement

Shohei Horike: Writing – review & editing, Writing – original draft, Resources, Methodology, Investigation, Funding acquisition, Formal analysis, Data curation, Conceptualization. **WEI QINGSHUO:** Writing – review & editing, Writing – original draft, Resources, Methodology, Investigation, Funding acquisition, Formal analysis, Data curation, Conceptualization.

Declaration of Competing Interest

The authors declare that they have no competing interests.

Acknowledgments

This research was partly supported by the A-STEP program of the Japan Science and Technology Agency under Grant Number JPMJTR23R6.

Appendix A. Supporting information

Supplementary data associated with this article can be found in the online version at doi:10.1016/j.synthmet.2026.118086.

Data availability

Data will be made available on request.

References

[1] S.G. Deng, H.L. Zhao, W.J. Fang, J.W. Yin, S. Dustdar, A.Y. Zomaya, Edge intelligence: the confluence of edge computing and artificial intelligence, IEEE Internet Things J. 7 (2020) 7457–7469, https://doi.org/10.1109/Jiot.2020.2984887.
[2] V. Pecunia, S.R.P. Silva, J.D. Phillips, E. Artegiani, A. Romeo, H. Shim, A.P. Joshi, Roadmap on energy harvesting materials, J. Phys. Mater. 6 (2023) 042501, https://doi.org/10.1088/2515-7639/acc550.
[3] G.J. Snyder, E.S. Toberer, Complex thermoelectric materials, Nat. Mater. 7 (2008) 105–114, https://doi.org/10.1038/nmat2090.
[4] T.J. Seebeck, Ueber die magnetische polarisation der Metalle und Erze durch temperatur-differenz, Ann. der Phys. 82 (1826) 133–160, https://doi.org/10.1002/andp.18260820202.

[5] G.J. Tan, L.D. Zhao, M.G. Kanatzidis, Rationally designing high-performance bulk thermoelectric materials, Chem. Rev. 116 (2016) 12123–12149, https://doi.org/10.1021/acs.chemrev.6b00255.
[6] B. Russ, A. Glaudell, J.J. Urban, M.L. Chabinyc, R.A. Segalman, Organic thermoelectric materials for energy harvesting and temperature control, Nat. Rev. Mater. 1 (2016) 16050, https://doi.org/10.1038/natrevmats.2016.50.
[7] Q. Wei, S. Horike, Advances in organic thermoelectric materials: from molecular design to device implementation, Inf. Funct. Mater. 2 (2025) 105–117, https://doi.org/10.1002/ifm2.33.
[8] J.L. Blackburn, A.J. Ferguson, C. Cho, J.C. Grunlan, Carbon-nanotube-based thermoelectric materials and devices, Adv. Mater. 30 (2018) 1704386, https://doi.org/10.1002/adma.201704386.
[9] X.Y. Wang, Y.F. Ding, X.Y. Zhang, Y.Y. Zhou, C.K. Pan, Y.H. Li, J. Pei, Light-triggered regionally controlled n-doping of organic semiconductors, Nature 642 (2025), https://doi.org/10.1038/s41586-025-09075-y.
[10] S.C. Wang, Y.T. Huang, B.Y. Zhao, S.Y. Lv, Y.L. Song, X.W. Xie, L. Wang, Green solvent-processed n-type fluorinated salt/single-walled carbon nanotube film with high performance for multifunctional wearable thermoelectric devices, J. Colloid Interface Sci. 705 (2026), https://doi.org/10.1016/j.jcis.2025.139512.
[11] R.S. Lee, H.J. Kim, J.E. Fischer, A. Thess, R.E. Smalley, Conductivity enhancement in single-walled carbon nanotube bundles doped with K and Br, Nature 388 (1997) 255–257, https://doi.org/10.1038/40822.
[12] C.M. Gao, Y.J. Liu, Y. Gao, Y. Zhou, X.Y. Zhou, X.J. Yin, L. Wang, High-performance n-type thermoelectric composites of acridones with tethered tertiary amines and carbon nanotubes, J. Mater. Chem. A 6 (2018) 20161–20169, https://doi.org/10.1039/c8ta08045c.
[13] M. Shim, A. Javey, N.W.S. Kam, H.J. Dai, Polymer functionalization for air-stable n-type carbon nanotube field-effect transistors, J. Am. Chem. Soc. 123 (2001) 11512–11513, https://doi.org/10.1021/ja0169670.
[14] Y. Nonoguchi, K. Ohashi, R. Kanazawa, K. Ashiba, K. Hata, T. Nakagawa, T. Kawai, Systematic conversion of single walled carbon nanotubes into n-type thermoelectric materials by molecular dopants, Sci. Rep. 3 (2013) 3344, https://doi.org/10.1038/srep03344.
[15] Y. Nonoguchi, M. Nakano, T. Murayama, H. Hagino, S. Hama, K. Miyazaki, T. Kawai, Simple salt-coordinated n-type nanocarbon materials stable in air, Adv. Funct. Mater. 26 (2016) 3021–3028, https://doi.org/10.1002/adfm.201600179.
[16] M. Mukaida, K. Kirihara, S. Horike, Q.S. Wei, Stable organic thermoelectric devices for self-powered sensor applications, J. Mater. Chem. A 8 (2020) 22544–22556, https://doi.org/10.1039/d0ta08598g.
[17] M. Mukaida, K. Kirihara, T. Ebihara, Q.S. Wei, Gram-scale polymer-based thermoelectric module for charging Li-ion batteries, Mater. Today Energy 32 (2023) 101238, https://doi.org/10.1016/j.mtener.2022.101238.
[18] T. Fujisaka, H. Sui, R.O. Suzuki, Design and numerical evaluation of cascade-type thermoelectric modules, J. Electron. Mater. 42 (2013) 1688–1696, https://doi.org/10.1007/s11664-012-2400-3.
[19] M. Nishinaka, Q. Wei, Y. Koshiba, S. Horike, n-Type carbon nanotubes doped by cross-linked organic superbase for stable thermoelectric materials, Energy Mater. Adv. 5 (2024), https://doi.org/10.34133/energymatadv.0123.
[20] S. Horike, Q.S. Wei, K. Akaike, K. Kirihara, M. Mukaida, Y. Koshiba, K. Ishida, Bicyclic-ring base doping induces n-type conduction in carbon nanotubes with outstanding thermal stability in air, Nat. Commun. 13 (2022) https://doi.org/ARTN351710.1038/s41467-022-31179-6.
[21] K. Kawasaki, I. Harada, K. Akaike, Q. Wei, Y. Koshiba, S. Horike, K. Ishida, Complex chemistry of carbon nanotubes toward efficient and stable p-type doping, Commun. Mater. 5 (2024), https://doi.org/10.1038/s43246-024-00460-0.
[22] M. Nishinaka, I. Harada, K. Akaike, Q.S. Wei, Y. Koshiba, S. Horike, K. Ishida, Electrochemical charge-carrier modulation of carbon nanotubes using ionic liquids derived from organic superbases for stable thermoelectric materials, Carbon 218 (2024), https://doi.org/10.1016/j.carbon.2023.118667.
[23] M. Nishinaka, Y. Koshiba, A. Akiyama, M. Funahashi, S. Horike, Electrolyte-based one-shot potential application with crosslinked superbase cation for thermally stable N-Type carbon nanotubes with tunable thermoelectric properties, Adv. Sustain. Syst. (2025) e00698, https://doi.org/10.1002/adsu.202500698.
[24] M. Mukaida, Q. Wei, T. Ishida, Polymer thermoelectric devices prepared by thermal lamination, Synth. Met. 225 (2017) 64–69, https://doi.org/10.1016/j.synthmet.2016.11.016.
[25] M. Mukaida, K. Kirihara, Q.S. Wei, Enhanced power output in polymer thermoelectric devices through thermal and electrical impedance matching, ACS Appl. Energy Mater. 2 (2019) 6973–6978, https://doi.org/10.1021/acsaem.9b01342.
[26] A.T. Burkov, A. Heinrich, P.P. Konstantinov, T. Nakama, K. Yagasaki, Experimental set-up for thermopower and resistivity measurements at 100–1300 K, Meas. Sci. Technol. 12 (2001) 264–272, https://doi.org/10.1088/0957-0233/12/3/304.
[27] G.K. Reeves, H.B. Harrison, Obtaining the specific contact resistance from transmission-line model measurements, IEEE Electron. Device Lett. 3 (1982) 111–113, https://doi.org/10.1109/Edl.1982.25502.
[28] L.M. Vikhor, L.I. Anatychuk, P.V. Gorskyi, Electrical resistance of metal contact to BiTe based thermoelectric legs, J. Appl. Phys. 126 (2019) 164503, https://doi.org/10.1063/1.5117183.
[29] H.N.S. Aldin, M.R. Ghods, F. Nayebipour, M.N. Torshiz, A comprehensive review of energy harvesting and routing strategies for IoT sensors sustainability and communication technology, Sens. Int. 5 (2024), https://doi.org/10.1016/j.sintl.2023.100258.